Supporting Information

Enhanced Photoelectrochemical Oxidation of Glycerol to Dihydroxyacetone Coupled with Hydrogen Generation via Acceerative Middle Hydroxyl Dehydrogenation over a Bi^0/Bi^{3+} Interface of Cascade Heterostructure

Xinyan Feng [a], Xuefan Feng [a], Fuqin Zhang[a]*

[a] Powder Metallurgy Research Institute, Central South University, Changsha 410083, PR China

* Corresponding authors: Fuqin Zhang, E-mail: zhangfuqin@csu.edu.cn

Experimental Section

Chemicals and materials

Ammonium metatungstate ($(NH_4)_6H_2W_{12}O_{40}•xH_2O$, AR, ≥99.5%), bismuth nitrate pentahydrate ($Bi(NO_3)_3•5H_2O$, AR, ≥99.0%), ammonium metavanadate (NH_4VO_3, AR, ≥99.5%) were purchased from Macklin Reagent Co., ltd. Sulfuric acid (H_2SO_4, AR, 98%), hydrogen nitrate (HNO_3, AR, 65-68%), hydrochloric acid (HCl, AR, 37%) sodium sulfate (Na_2SO_4, AR, ≥99.5%), oxalic acid ($C_2H_2O_4$, AR, ≥99.5%) citric acid ($C_6H_8O_7$, AR, ≥99.5%), and hydrazine hydrate were obtained from Sinopharm Chemical Reagent Co., Ltd. All the reagents were used without further purification.

PEC performance for photoanodes

The PEC performance was performed on an electrochemical workstation (CHI760E), the electrolyte was 0.5 M Na_2SO_4 mixed with 0.1 M glycerol electrolyte with pH adjusted to 2 by H_2SO_4, the light source was a 300 W Xe lamp (CEL-PF300-T8) with an AM 1.5G filter, and the standard three-electrode configuration consisted of a working electrode (as-prepared photoanodes), a counter electrode (platinum foil) and a reference electrode (Ag/AgCl electrode).

Electrochemical impedance spectroscopy (EIS) was employed to determine the charge carrier mobility. EIS spectra were monitored with 5 mV AC voltage amplitude, where the frequency range was set to be 0.1-10^6Hz. The transient photocurrent response was performed without bias voltage under irradiation of a xenon lamp with an interval of 30 s for light on and off. Mott-Schottky (MS) curves were collected at the amplitude of 5 mV scanning from -0.5 V to 0.5 V (vs. Ag/AgCl) with a 1000 Hz frequency under dark condition.

The reversible hydrogen electrode (RHE) potentials were converted from the measured potentials according to the followed equation:

$$E_{RHE} = E_{Ag/AgCl} + E_{Ag/AgClvs.NHE} + 0.059 \times pH \quad (1)$$

where $E_{Ag/AgClvs.NHE}$ is 0.197 V at 25 °C.

Selectivity of DHA was calculated by:

$$\text{Selectivity (DHA)} = c_{DHA}/(c_{DHA} + c_{GLD} + c_{GA} + c_{FA}) \times 100\% \quad (2)$$

Faradaic efficiency was calculated by:

$$\text{Faradaic efficiency} = e_{products} \times n_{products} \times N/(Q/n) \times 100\% \quad (3)$$

where $e_{products}$ is the number of holes required to oxidize glycerol molecule to products, including DHA ($e = 2$), GLD ($e = 2$), GA ($e = 2$), FA ($e = 8$), $n_{products}$ is the productivity of products, N is Avogadro's constant ($N = 6.02 \times 10^{23}$), Q is the quantity of electric charge, and n is the elementary charge ($e = 1.602 \times 10^{-19}$C).

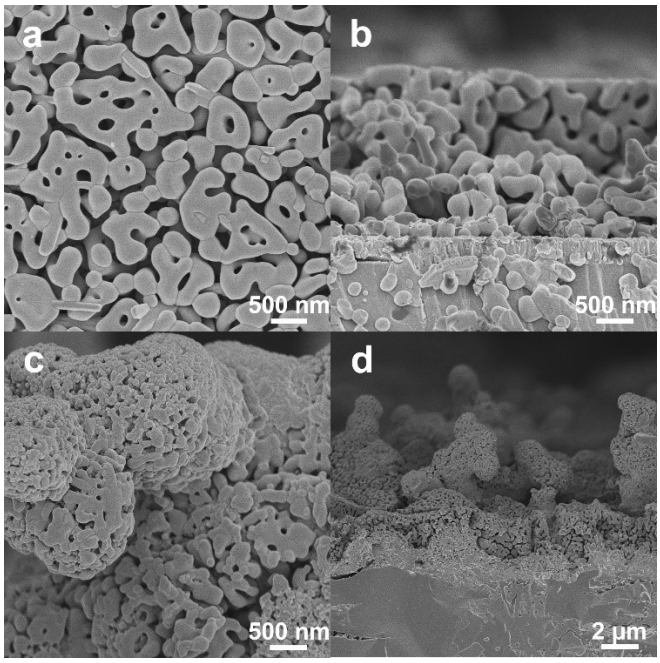

Fig. S1. (a) SEM image of $BiVO_4$ (top-view). (b) SEM image of $BiVO_4$ (cross-view). (c) SEM image of $WO_3/BiVO_4$ (top-view). (d) SEM image of $WO_3/BiVO_4$ (cross-view).

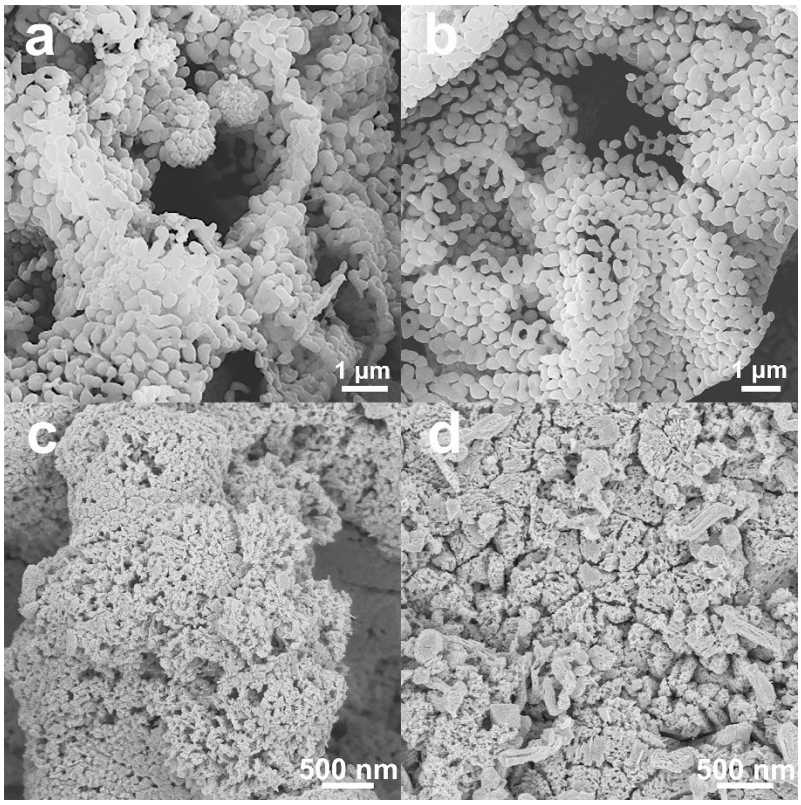

Fig. S2. (a) Top-view SEM image of $WO_3/BiVO_4$-30. (b) Top-view SEM image of $WO_3/BiVO_4$-40. (c) Top-view SEM image of $WO_3/BiVO_4$/Bi-0.15%. (d) Top-view SEM image of $WO_3/BiVO_4$/Bi-0.20%.

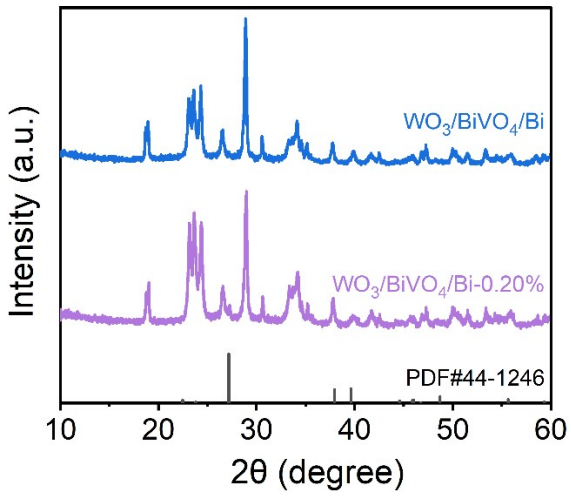

Fig. S3. XRD patterns of $WO_3/BiVO_4$/Bi and $WO_3/BiVO_4$/Bi-0.20%.

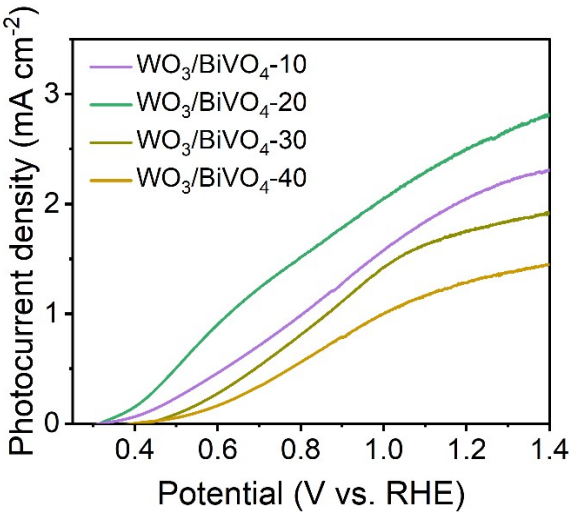

Fig. S4. LSV curves of $WO_3/BiVO_4$-10, $WO_3/BiVO_4$-20 ($WO_3/BiVO_4$), $WO_3/BiVO_4$-30 and $WO_3/BiVO_4$-40 photoanodes.

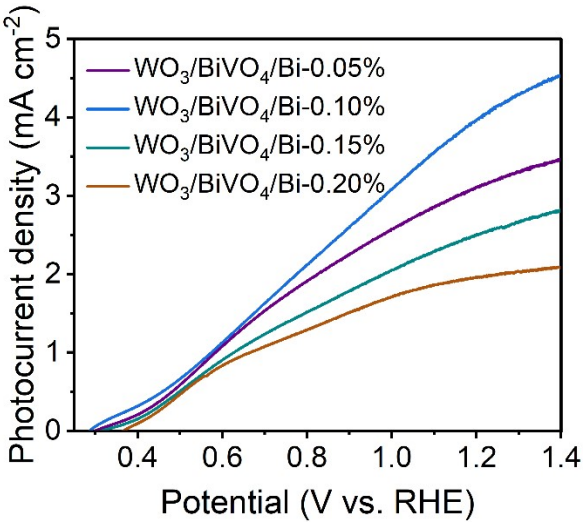

Fig. S5. LSV curves of $WO_3/BiVO_4/Bi$-0.05%, $WO_3/BiVO_4/Bi$-0.10% ($WO_3/BiVO_4/Bi$), $WO_3/BiVO_4/Bi$-0.15% and $WO_3/BiVO_4/Bi$-0.20% photoanodes.

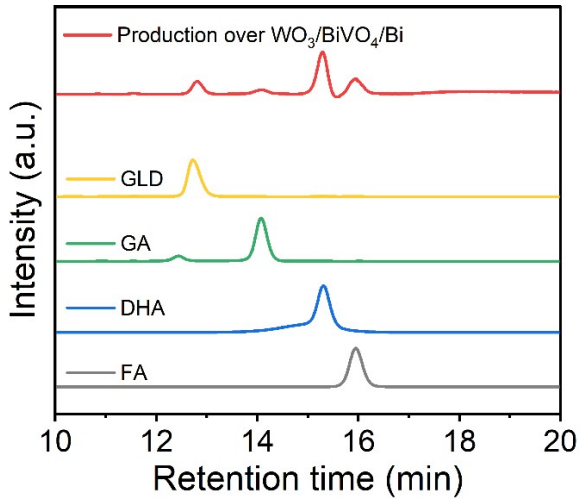

Fig. S6. High performance liquid chromatography (HPLC, UV detector = 210 nm) spectra of the PEC glycerol oxidation products over $WO_3/BiVO_4/Bi$ photoanode for 1 h.

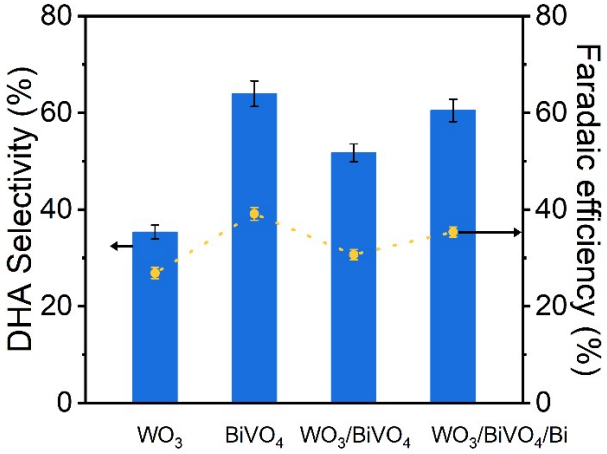

Fig. S7. DHA selectivity and faradaic efficiency in 0.5 M Na_2SO_4 (pH = 2) with 0.1 M glycerol over WO_3, $BiVO_4$, $WO_3/BiVO_4$ and $WO_3/BiVO_4/Bi$ photoanodes at 1.2 V vs. RHE under AM 1.5G illumination (100 mW cm^{-2}).

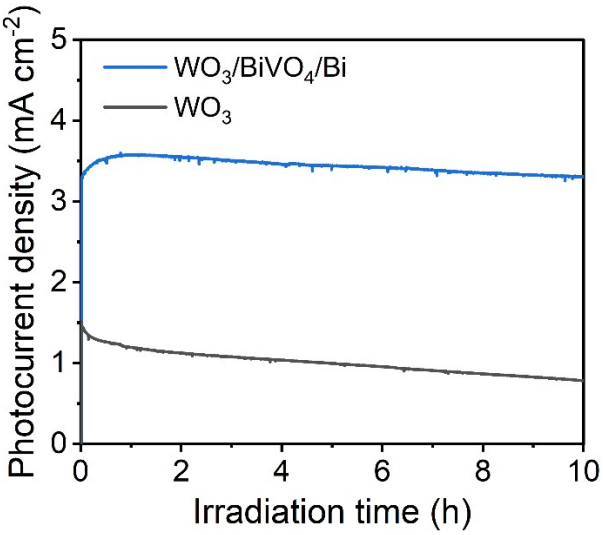

Fig. S8. *J-t* stability tests of WO_3 and $WO_3/BiVO_4/Bi$ photoanodes measured at 1.2 V vs. RHE for 10 h.

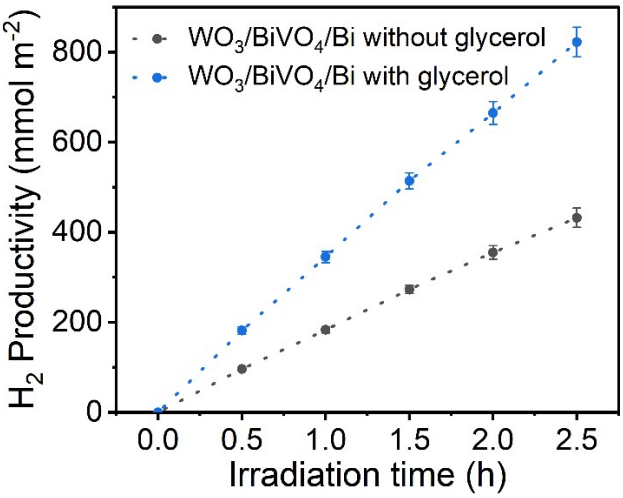

Fig. S9. H_2 productivity in the $WO_3/BiVO_4/Bi$-Pt tandem cell measured at 1.2 V vs. RHE with and without glycerol.

Table S1. Bi element contents of electrolyte after reaction for 1 h, 5 h and 10 h by inductively coupled plasma-atomic emission spectroscopy (ICP-AES).

Sample	Bi content (%)
electrolyte (1 h)	<0.0001%
electrolyte (5 h)	<0.0001%
electrolyte (10 h)	<0.0001%

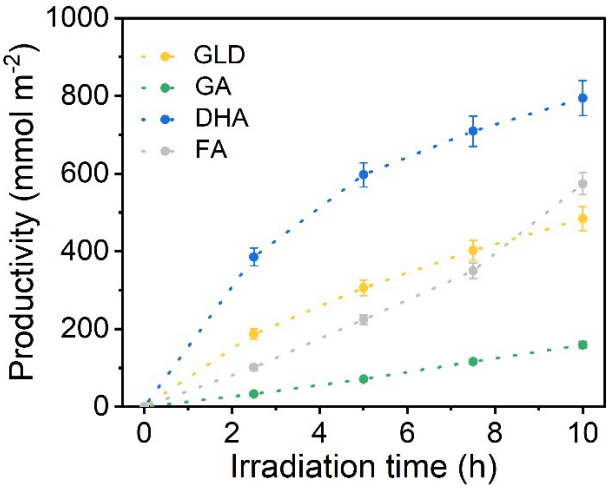

Fig. S10. Productivity of products in the $WO_3/BiVO_4$/Bi-Pt tandem cell measured at 1.2 V vs. RHE for 10 h.

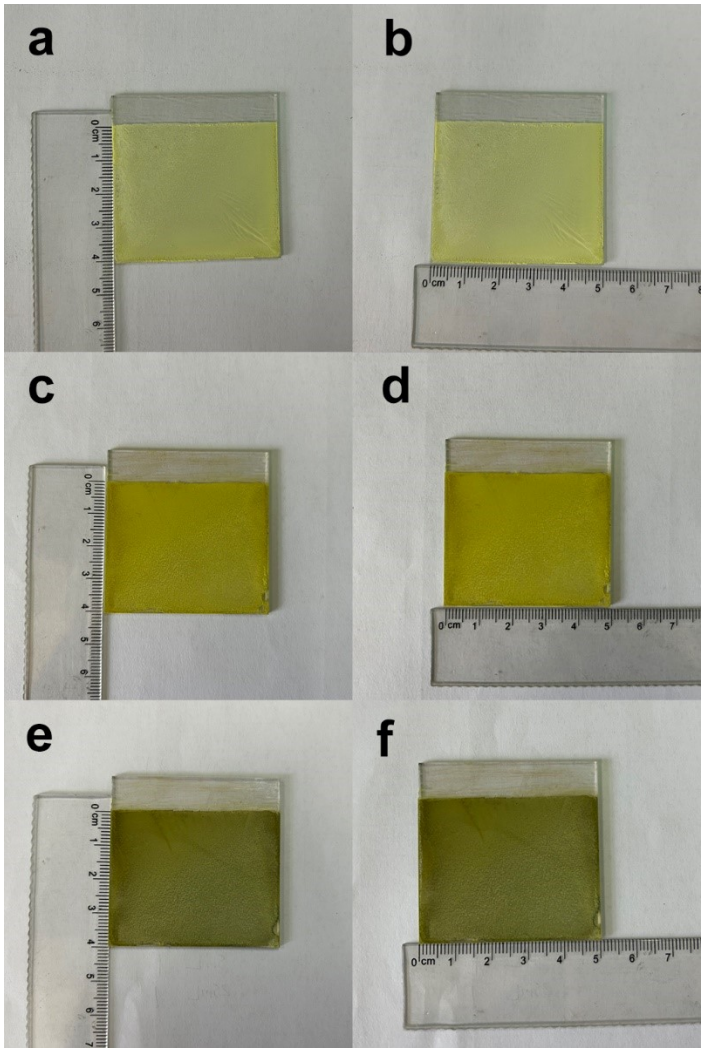

Fig. S11. Photographs of the the large size (5 × 4 cm^2) photoanodes. (a, b) WO_3 photoanode (c, d) $WO_3/BiVO_4$ photoanode (e, f) $WO_3/BiVO_4$/Bi photoanode.

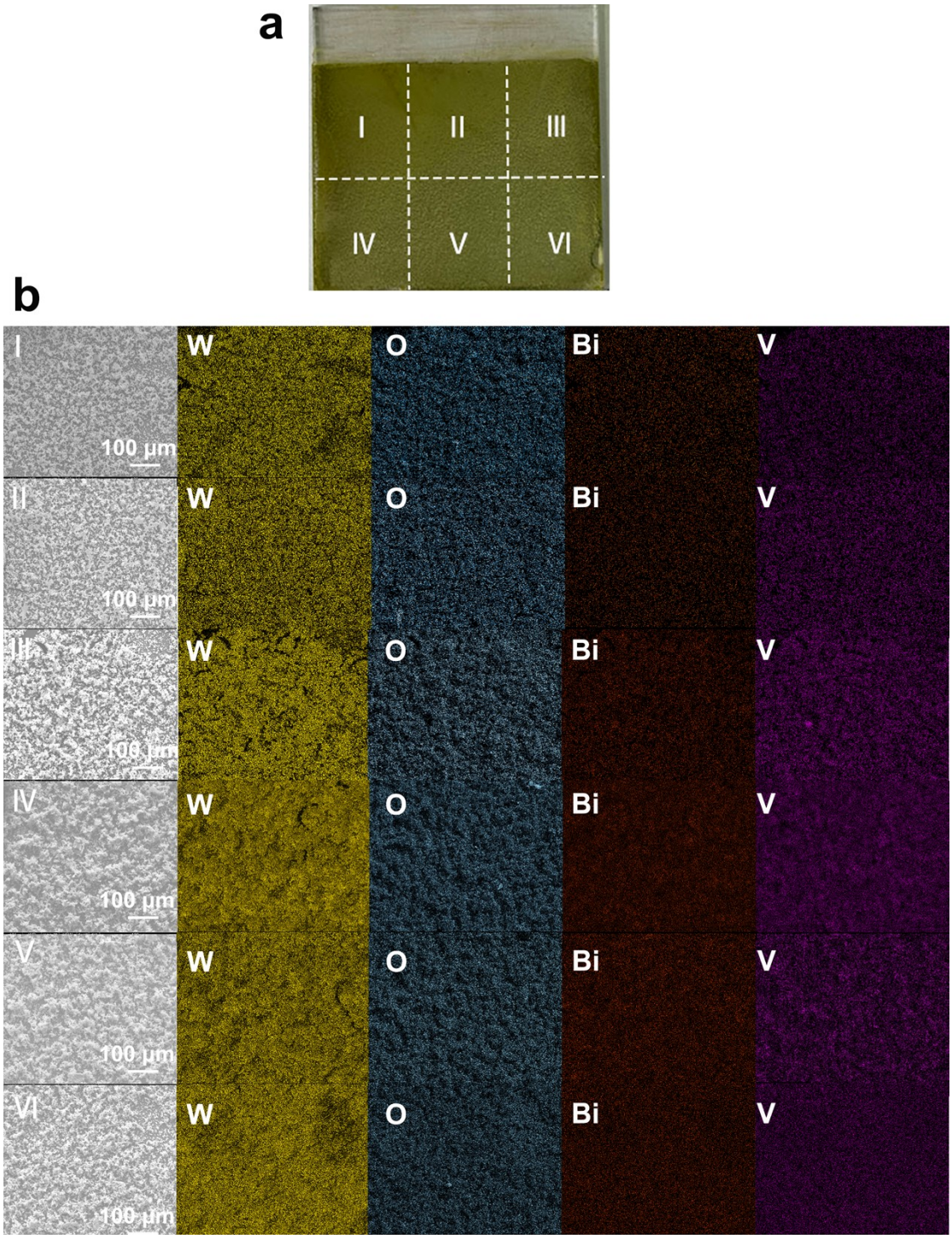

Fig. S12. (a) Photograph of the the large size $WO_3/BiVO_4/Bi$ photoanodes (divided into 6 areas). (b) SEM and corresponding element mapping images in the above six areas.

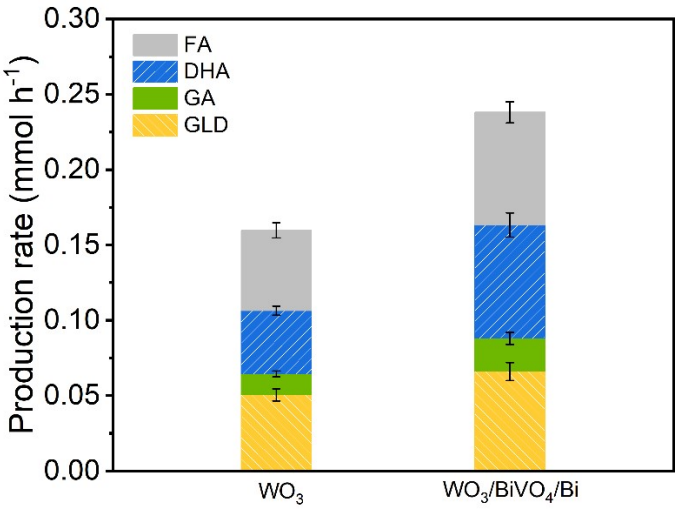

Fig. S13. Photoelectrocatalytic production rate of oxidation products on large-sized as-prepared photoanodes.

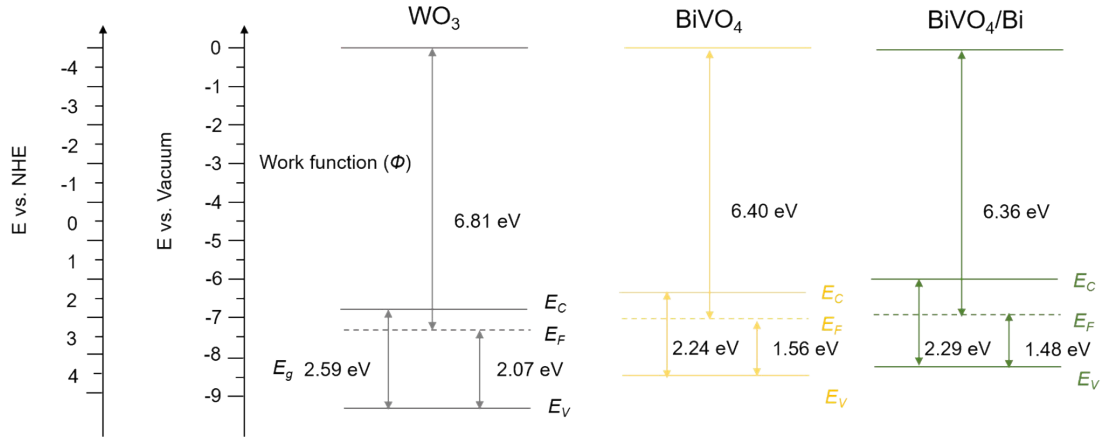

Fig. S14. Schematic energy band diagrams of WO_3, $BiVO_4$ and $BiVO_4$/Bi before contact. E_g, band gap; E_F, Fermi level; E_C, conduction band position; E_V, valence band position.